Maastricht University

Stability of samples in coating research: From edge effect to ageing

Citation for published version (APA):

Lumaca, D., Amato, A., Bischi, M., Cagnoli, G., Cesarini, E., Fafone, V., Granata, M., Guidi, G. M., Lorenzini, M., Martelli, F., Mereni, L., Minenkov, Y., Montani, M., Nardecchia, I., Piergiovanni, F., Placidi, E., & Rocchi, A. (2023). Stability of samples in coating research: From edge effect to ageing. *Journal of Alloys and Compounds*, *930*, Article 167320. https://doi.org/10.1016/j.jallcom.2022.167320

Document status and date:
Published: 05/01/2023

DOI:
10.1016/j.jallcom.2022.167320

Document Version:
Publisher's PDF, also known as Version of record

Document license:
Taverne

Please check the document version of this publication:

• A submitted manuscript is the version of the article upon submission and before peer-review. There can be important differences between the submitted version and the official published version of record. People interested in the research are advised to contact the author for the final version of the publication, or visit the DOI to the publisher's website.
• The final author version and the galley proof are versions of the publication after peer review.
• The final published version features the final layout of the paper including the volume, issue and page numbers.

Link to publication

General rights
Copyright and moral rights for the publications made accessible in the public portal are retained by the authors and/or other copyright owners and it is a condition of accessing publications that users recognise and abide by the legal requirements associated with these rights.

• Users may download and print one copy of any publication from the public portal for the purpose of private study or research.
• You may not further distribute the material or use it for any profit-making activity or commercial gain
• You may freely distribute the URL identifying the publication in the public portal.

If the publication is distributed under the terms of Article 25fa of the Dutch Copyright Act, indicated by the “Taverne” license above, please follow below link for the End User Agreement:

www.umlib.nl/taverne-license

Take down policy
If you believe that this document breaches copyright please contact us at:

repository@maastrichtuniversity.nl

providing details and we will investigate your claim.

Download date: 24 Apr. 2024

Journal of Alloys and Compounds 930 (2023) 167320

Contents lists available at ScienceDirect

Journal of Alloys and Compounds

journal homepage: www.elsevier.com/locate/jalcom

Stability of samples in coating research: From edge effect to ageing

Diana Lumaca [a,b,*], Alex Amato [c,d], Matteo Bischi [e], Gianpietro Cagnoli [f], Elisabetta Cesarini [b], Viviana Fafone [a,b], Massimo Granata [g], Gianluca Maria Guidi [e], Matteo Lorenzini [a,b], Filippo Martelli [e], Lorenzo Mereni [g], Yury Minenkov [b], Matteo Montani [e], Ilaria Nardecchia [b], Francesco Piergiovanni [e], Ernesto Placidi [h], Alessio Rocchi [b]

[a] Università degli Studi di Roma Tor Vergata, Roma I-00133, Italy
[b] Istituto Nazionale di Fisica Nucleare, Sez. di Roma Tor Vergata, Roma I-00133, Italy
[c] Maastricht University, Maastricht N-6200, the Netherlands
[d] Nikhef, Amsterdam N-1098, the Netherlands
[e] Università degli Studi di Urbino Carlo Bo, Urbino I-61029, Italy
[f] Université de Lyon, Université Claude Bernard Lyon 1, CNRS, Institut Lumière Matière, Villeurbanne F-69622, France
[g] Laboratoire des Matériaux Avancés - IP2I, CNRS, Université de Lyon, Université Claude Bernard Lyon 1, Villeurbanne F-69622, France
[h] Sapienza Università di Roma, Roma I-00185, Italy

ARTICLE INFO

Article history:
Received 30 April 2022
Received in revised form 16 September 2022
Accepted 21 September 2022
Available online 28 September 2022

Keywords:
Amorphous materials
Oxide materials
Laser processing
Elasticity
Impurities in semiconductors
Mechanical properties

ABSTRACT

Mechanical and optical thermal noises play an important role in many precise opto-mechanical experiments, in which positions of test bodies are monitored by laser beams. Much of the research in this area was driven by the physics of gravitational wave interferometers, to counteract the mirror's multi-layered dielectric coating thermal noise. Coating thermal noise is directly related to structural dissipation inside the material through the loss angle. In view of future upgrades of gravitational wave detectors, increasing the coatings mechanical performances, by lowering the loss angle and retaining their outstanding optical and morphological properties, is fundamental. The measurement of the coating loss angle requires substrates to be stable with respect to their dissipative behavior. It has been seen that fused silica disc losses are resonant-mode shape dependent and are subject to ageing effects, compromising the accuracy of mechanical characterizations of the substrates and, consequently, of the coatings. In commercial samples, the source of this deteriorations can be related to the ground, unpolished lateral surface. In this work we show that the polishing of the sample's edge reduces the amount of spurious losses and ageing effects. A new procedure through CO_2 laser polishing of the edge surface is proposed, explained and put in place. The results of these procedures, in terms of roughness and loss behavior is shown. The loss angle measurements are compared with an edge loss model and other existing models.

© 2022 Elsevier B.V. All rights reserved.

1. Introduction

Thermal noise (TN) due to multi-layer dielectric coatings plays an important role in many precise opto-mechanical experiments that use high-finesse optical cavities, such as frequency standards for laser stabilization, quantum computing devices and opto-mechanical resonators [1–3]. Much of the experimental and theoretical research on TN reduction was driven by the physics of gravitational wave interferometric detectors, where the frequency band between 10 and 300 Hz is currently limited by the Brownian TN arising from thermally-driven fluctuations of atoms in multi-layer reflective coatings deposited on the mirror test masses. The reduction of this noise is fundamental for advanced detectors and all high precision measurement experiments.

The level of a system's Brownian TN is linked via the Fluctuation-Dissipation theorem [4] to the dissipative dynamic of the observable chosen for the description of the system itself. In our case the observable q is the mirror front face displacement averaged over the laser beam profile: q is the single valued quantity sensed by the interferometer.

Following the work carried out by Levin [5] it is possible to derive the TN of the observable q through the energy dissipation of an harmonic external force $\vec{F}(t)$ acting on the mirror front face and having a surface distribution (pressure) exactly equal to that of the

* Corresponding author at: Università degli Studi di Roma Tor Vergata, Roma I-00133, Italy.
E-mail address: diana.lumaca@roma2.infn.it (D. Lumaca).

https://doi.org/10.1016/j.jallcom.2022.167320
0925-8388/© 2022 Elsevier B.V. All rights reserved.

laser beam. The power spectral density S_{qq} of the TN associated to the displacement is:

$$S_{qq}(\omega) = \frac{8k_B T}{\omega^2}\frac{<W_{diss}>}{F_0^2}, \tag{1}$$

where k_B is the Boltzman constant, T is the system's temperature, ω is the frequency, F_0 is the amplitude of the external applied force, $< W_{diss} >$ is the power dissipated by the external force, averaged over one period. If no dissipation is present then that averaged power is zero. $< W_{diss} >$ can be evaluated once the dissipative processes are known; for the important case of the structural damping, one can write in general:

$$<W_{diss}> = 2\pi f U_{max}\phi(\omega), \tag{2}$$

where U_{max} is the energy of elastic deformation when the test mass is maximally contracted or extended under the action of the external force, and $\phi(\omega)$ is the dissipation's loss angle, that is, a damping coefficient. Internal damping effects (i.e. internal frictions) arise from the anelasticity of the system itself: when a stress is applied, the strain response is not instantaneous, it is characterized by a finite relaxation time. The stress-strain phase lag is the loss angle ϕ and it is related to the dissipated energy E_{diss} in one cycle by ($E_{diss} = f < W_{diss} >$):

$$\phi(\omega) = \frac{1}{2\pi}\frac{E_{diss}}{E_{tot}}. \tag{3}$$

The loss angle at resonance frequency corresponds to the inverse of the mechanical quality factor $\phi(\omega_0) = 1/Q$.

Following the work by Levin, *TN of the mirrors and coating for the gravitational waves detector* specific case can be extrapolated as:

$$S_{TN}(f) \sim \frac{2k_B T}{\sqrt{\pi^3 f}}\frac{1-\sigma s^2}{wY_s}\left(\phi_s + \frac{2}{\sqrt{\pi}}\frac{1-2\sigma_s}{1-\sigma_s}\frac{t_c}{w}\phi_c\right), \tag{4}$$

where w is the radius of the laser beam at the mirror surface, Y_s and σ_s are respectively substrate's material Young's modulus and Poisson's ratio and t_c is the coating thickness, and ϕ_s and ϕ_c are respectively the substrate's and coating's loss angles. The dominant part is due to internal friction inside the highly reflective coating materials, since the bulk loss angle is more than four orders of magnitude smaller than that of the coatings [6]. To reduce the *Coating Thermal Noise (CTN)*, one can act on temperature (going cryogenic), coating optical thickness (looking for coating materials that allows to increase the refractive index contrast and reduce layer numbers and coating overall thickness, maintaining the same level of total reflectivity), laser spot dimension (to be increased), and finally coating loss angle ϕ_c (to be reduced using low-loss materials).

Measuring the mechanical dissipation in coatings is not trivial. In general, the coating loss angle ϕ_c can be worked out looking at its effects on the loss of the substrate it is deposited on. Considering the coated sample as a system composed of the substrate and the coating film, each with some energy stored in it, depending on the material properties and dimensions; the coating loss angle can be calculated through the balance of dissipated energy [7]:

$$\phi_{tot} = D\phi_c + (1-D)\phi_s \tag{5}$$

where ϕ_{tot} is the loss angles of the coated sample and $D = E_c/E_{tot}$ is the dilution factor, defined as the ratio between the energy stored in the coating with respect to the total one. It can be evaluated by computation through analytical method or finite elements analysis, or it can be measured through the frequency shift of resonance modes before and after coating deposition [8]:

$$D \simeq 1 - \left(\frac{f_s}{f_{tot}}\right)^2\frac{m_s}{m_{tot}}, \tag{6}$$

where f_s and f_{tot} are the resonance frequencies before and after coating deposition and m_s and m_{tot} are the masses of the sample before and after coating deposition.

This estimation is important because it gives a *direct* measurement of the dilution factor D, independent from assumptions regarding material visco-elastic parameters, needed for computational methods. It must be noted that the previous expression is valid only if the coating is deposited uniformly over the sample and its thickness is small enough to not change significantly the shape of the mode.

The measurement of the dilution factor gives also the opportunity to work out the elastic constants of coatings, once the physical dimensions are known. Following the analytical derivation of the elastic energies [9]:

$$D^{-1} = \frac{E_{tot}}{E_c} \simeq \frac{Y_s t_s}{3Y_c t_c}. \tag{7}$$

Equations (5) and (7) clearly show that the knowledge of the properties of coatings is relative to that of the substrates. Any uncertainty in the mechanical characterization of substrates will be transferred to that of coatings. In particular, from equation (5), the relative uncertainty of the substrate loss angles is multiplied by 1/D before giving the relative uncertainty of the coating loss angle.

Disc-shaped samples can be used to make mechanical characterizations through the ring-down resonant method and a *Gentle Nodal Suspension (GeNS)*, that is nowadays considered one of the most power-full tool to work out loss angle of coating materials, due to its high reproducibility and the ultra high decoupling of modes to the suspension system [10]. A GeNS setup able to measure disc-shaped samples down to 1″ diameter at room temperature is located at Roma Tor Vergata INFN laboratory (see Fig. 1) and is the one used to perform all the mechanical characterizations shown in the following sections.

To appropriately characterize the coating loss angle, the knowledge of the substrate mechanical behavior and its stability are fundamental. In the following sections, we will show that SiO_2 disc-shaped resonators, frequently used for this purpose, show some peculiar loss angle's behaviors that must be taken in consideration; the experimental data will be justified by a model considering spurious surface losses arising from unpolished sample's edge and a technique to treat the sample's edge surface will be presented and characterized.

2. Losses behavior in SiO_2 resonators

Fused silica is the material currently used for gravitational waves interferometer mirrors, because of its very low loss angle at room temperature ($\phi_{SiO_2} \sim 10^{-9}$ [6]). For the same reason, together with its cheap price and the ease with which can be found on the market, fused silica disc-shaped resonators are also widely used in CTN research.

These substrates have always shown a peculiar behavior in the mechanical losses distribution. Contrary to what it is expected in an homogeneous resonator, the measured loss angle shows a strong dependence on the mode shape. Modes are organized in families: drum, butterfly and different order of mixed modes[1] [11] (see Fig. 2) follow separated continuous lines, generating a family branching in the losses. Furthermore, these substrates also suffer loss angle *variation over time* due to ageing effects and possible absorption of contaminants, especially through the lateral surface.

[1] Mode families of disc-shaped resonators are ordered through azimuthal and radial nodal line numbers, m and n respectively. In this way it is possible to identify pure radial (drum), pure azimuthal (butterfly) and mixed modes.

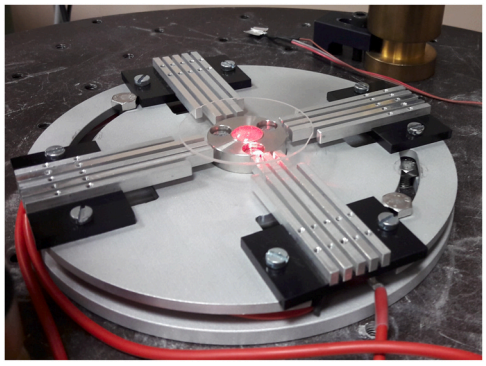

Fig. 1. GeNS setup located at Roma Tor Vergata INFN laboratory. A 2" diameter and 1 mm thickness disc is shown. The red color comes from the laser used to detect the vibrations. The system can measure discs of diameter up to 3". The four sets of 5 aluminium rods are used to excite the disc modes through high voltage AC potential.

Fig. 3 shows an example of both these effects [12]: the loss angles of just two families are reported and the existence of the two relative branches is evident; furthermore, starting from the initial characterization (blue circles) the mechanical losses get worse in a following measurement after 55 days (red squares); this effect can be healed through an annealing at high temperature (green triangles), but the treatment is not definitive, because the losses get worse again after other 68 days (yellow diamonds).

These two issues make the mechanical characterization of the SiO_2 substrates not so trivial. In the following sections these behaviors are shown and modelled through two different theoretical models; in A there is an evaluation of the effect of substrate loss variation on coating loss angle detectability.

2.1. Mode dependence

A possible reason to the mode dependence distribution is described by a *bulk and shear model* [13,14]: historically this model with two loss angles was used to fit coating's losses, but also substrate's ones.

Another possible reason is described by a *surface loss model* [11], according to which spurious losses can arise from rough not polished barrel of the samples.

In the following, both of them are briefly exposed and applied to the same experimental data set: loss angle measurements of a commercial disc-shaped sample made of Corning®7980, 1″ diameter and 0.5 mm thickness, with rough edge surface.

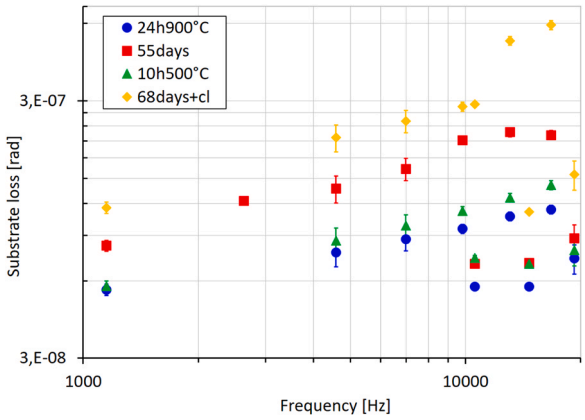

Fig. 3. Loss angle dependence on mode families [12] for a Corning®7980 sample of 3″ diameter and 1 mm thickness. Blue circles are the initial mechanical characterization. Red square show the ageing effect in a following measurement performed 55 days after. Green triangles are the characterization after an annealing treatment. The yellow diamonds are the last characterization, 68 days after the previous one, that shows that the annealing does not stop ageing effects definitively.

2.1.1. Bulk and shear

Following the theory presented in [13], the loss angle is given by a combination of ϕ_{bulk} and ϕ_{shear}:

$$\phi_{tot} = \frac{U_{bulk}}{U_{tot}}\phi_{bulk} + \frac{U_{shear}}{U_{tot}}\phi_{shear} = D_{bulk}\phi_{bulk} + D_{shear}\phi_{shear}, \tag{8}$$

where D_{bulk} and D_{shear} are the dilution factors of the bulk and shear deformations. Their explicit expression is really complex even for thin, homogeneous and isotropic membranes [15,16] and depends on the Poisson's ratio and the deformed shape of the membrane.

For the two loss angles, a power law frequency dependence can be adopted [17,18] (although this dependence has been verified in silica only at temperatures between 20 K and 110 K):

$$\phi_{bulk} = Af^B, \tag{9}$$

$$\phi_{shear} = Cf^D, \tag{10}$$

where A, B, C and D are the parameters to be estimated. The total loss angle becomes:

$$\phi_{tot} = D_{bulk}Af^B + D_{shear}Cf^D. \tag{11}$$

In Tab. 1 and Fig. 4, D_{bulk} and D_{shear} values are computed for the specific case of the SiO_2 thin disc approximation, for a series of resonant modes: the values of D_{bulk} are evaluated on the basis of eq. 24 in [15]. D_{shear} is calculated as $1 - D_{bulk}$. The resonant modes of disc-

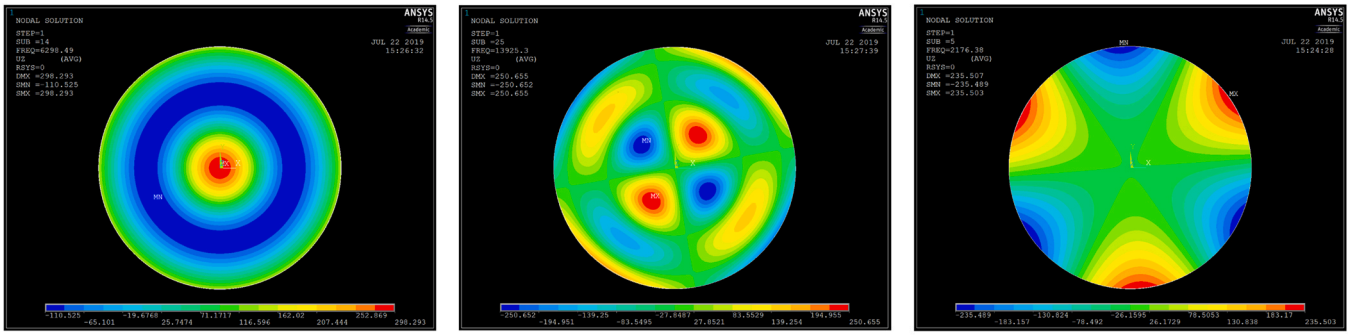

Fig. 2. Example of three disc-shaped resonators excitation modes: (a) pure drum mode (0,2), with 2 radial nodal lines (it cannot be measured with GeNS); (b) mixed mode (2,2), with 2 azimuthal and 2 radial nodal lines; (c) pure butterfly mode (3,0), with 3 azimuthal nodal lines. Simulated through *Ansys*®.

Table 1
Tables of the bulk and shear dilution factors for a fused silica SiO2 (Young modulus Y = 72.7 GPa, density $\rho = 2.201 \times 10^3$ kg/m^3, Poisson's ratio $\sigma = 0.16$) disc-shaped resonator, of 0.5 mm of thickness.

	D_{bulk}			D_{shear}		
m \ n	0	1	2	0	1	2
2	0.0695	0.3045	0.3154	0.9305	0.6955	0.6846
3	0.1100	0.2851	0.3068	0.8900	0.7149	0.6932
4	0.1372	0.2759	0.3009	0.8628	0.7241	0.6991
5	0.1568	0.2714	0.2968	0.8432	0.7286	0.7032
6	0.1716	0.2694	0.2939	0.8284	0.7306	0.7061
7	0.1842	0.2687	0.2919	0.8158	0.7313	0.7081
8	0.1932	0.2688	0.2906	0.8068	0.7312	0.7094
9	0.2009	0.2694	0.2896	0.7991	0.7306	0.7104
10	0.2078	0.2702	0.2891	0.7922	0.7298	0.7109

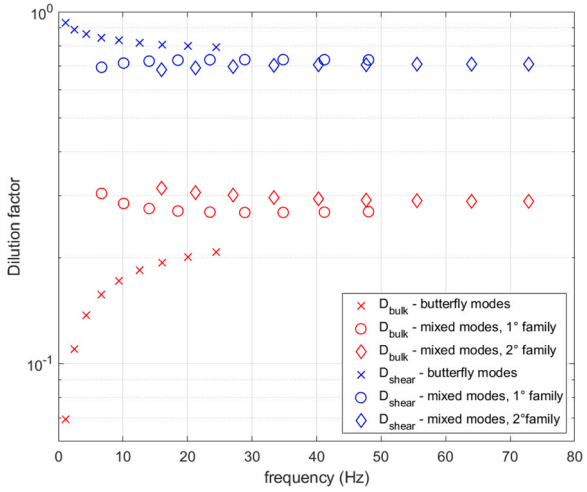

Fig. 4. Bulk and shear dilution factors of different modes. The Dilution factors are divided into families: crosses represent pure butterfly modes, circles represent mixed modes with one radial nodal line, diamonds represent mixed modes with two radial nodal lines.

shaped samples are ordered through azimuthal and radial nodal line numbers, represented usually by m and n respectively: Tab. 1 is organized following this classification, on the first column the number of azimuthal nodal lines are listed, on the first row the number of radial nodal lines are reported, both for bulk and shear dilution factors.

In Fig. 5, the comparison between experimental mechanical loss values of one of the samples studied in this work with an analytic expression provided by the bulk and shear model (eq. (11)) is reported. Looking at the experimental data (black stars) and considering that on the abscissa are reported the loss angles divided by D_{shear} for each mode, it is evident that the bulk contribution should be negligible with respect to the shear one. Looking at eq. (11), it should be $A \ll C$; for simplicity $A = 0$ it is assumed, and therefore:

$$\phi_{tot} \simeq D_{shear} C f^D. \tag{12}$$

Using values in Tab. 1, it is possible to obtain the reduced value:

$$R = \frac{\phi_{tot}}{D_{shear}} \simeq C f^D, \tag{13}$$

to be fitted just with a power law.

As can be seen in Fig. 5, the reduced values are still not placed all on a power law: the mixed mode (2,1) is still out of the butterfly modes behavior and to obtain a fit with a better R-square value, it must be excluded.

Therefore, the bulk and shear model is not able to reproduce all the experimental data, especially the mixed mode loss (separated with respect to the butterfly ones because of the family branching

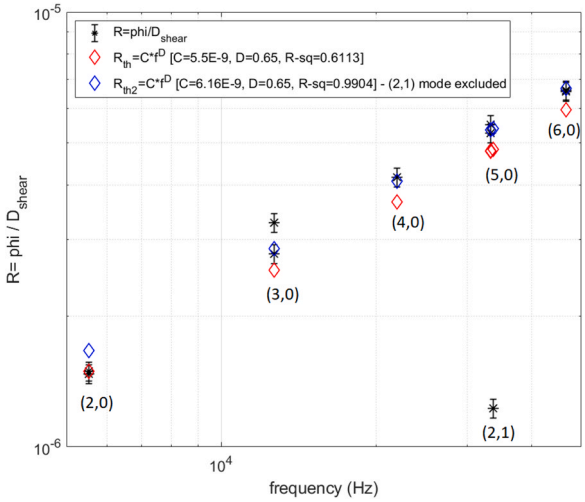

Fig. 5. Comparison between experimental reduced value (that is loss angle measurements divided by the dilution factor D_{shear}, see Eq.(13) (black stars); the *bulk and shear model* estimation (red diamond) fitted to all the data; the fit represented by the blue diamonds is the more suitable model, obtained excluding the mixed mode (2,1).

mentioned above); for this reason, at the moment, this model cannot be considered the best model to fit loss angle data for SiO_2 substrates.

2.1.2. Surface losses

An alternative model to explain the loss angle family branching is based on the evidence that butterfly modes store more elastic energy in the edge of the disc-shaped samples, with respect to mixed ones; the increased loss angle values observed for these modes can be due to surface losses.

In [11] the *surface loss model* justifies the existence of family branching and predicts the level of losses in disc-shaped resonators made of silica, silicon and brass. The peculiar losses distribution in SiO_2 substrates can be due to an *edge effect*, that arises from excess losses inside the rough, not polished edge of commercial samples. A relevant amount of energy would be dissipated in the thin, ground layer close to the surface and the actual energy lost would depend on the deformation induced at the disc edge, therefore it would be different for different mode shapes and, presumably, follow a branched trend depending on the mode family.

The model considers the disc-shaped resonator system as composed of two parts: the body and the lateral surface; furthermore, it considers only structural losses associated with the elastic energy stored in both parts. The dilution factor density ϵ is defined as the ratio between the elastic energy stored in the edge E_{edge} of thickness d and the total energy E_{tot}:

$$\epsilon = \lim_{d \to 0} \frac{1}{d} \frac{E_{edge}}{E_{tot}}. \tag{14}$$

As far as $d << r_0$, where r_0 is the resonator's radius (see Fig. 6), the dilution factor is therefore:

$$D_{edge} = \frac{E_{edge}}{E_{tot}} = \epsilon d. \tag{15}$$

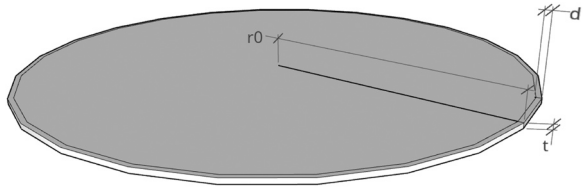

Fig. 6. Model of disc-shaped resonators.

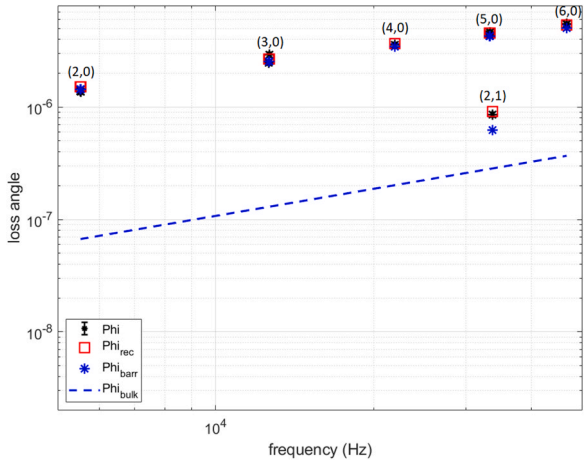

Fig. 7. Comparison between loss angle measurements (black stars) and *surface losses model* estimation (red square). Also the body (red dashed line) and edge (blue stars) contributions are highlighted.

The total loss angle of the system can be written as:

$$\phi_{\text{tot}} = D_{\text{body}}\phi_{\text{body}} + D_{\text{edge}}\phi_{\text{edge}} \simeq \phi_{\text{body}} + D_{\text{edge}}\phi_{\text{edge}}. \quad (16)$$

Since the body and the edge compose the whole disc system, then $D_{\text{edge}} + D_{\text{body}} = 1$. The above approximation holds when $D_{\text{edge}} << D_{\text{body}}$, which is our case since d is small.

For the body loss a power law frequency dependence can be assumed [17] and the expression for the total loss angle becomes:

$$\phi_{\text{tot}} = Af^{B} + \epsilon d\phi_{\text{edge}} = \phi_{\text{body}} + \phi_{\text{barrel}} \quad (17)$$

being ϕ_{body} and ϕ_{barrel} the two mechanical losses components.

In [11], numerical computations of ϵ values for Corning® samples normal modes up to $n = 8$ and $m = 2$ have been performed and finite element method (FEM) simulations of fused silica disc natural frequencies have been worked out, to perform the identification of the mode shapes for the measured modes.

In Fig. 7 the comparison between experimental loss values with an analytic expression of the same sample mentioned above is shown. In this particular case, it is easy to see that the barrel contribution (blue stars) to the mechanical losses of the disc are dominant with respect to the body one (blue-dashed line).

The described model reproduces all the observed mechanical losses with success, giving a strong indication that the branching of mechanical loss in mode families is related to the unpolished lateral surface of the disc.

It is worth mentioning that the same model can be implemented also to reproduce the losses of SiO_2 coating films (see [19]).

2.2. Ageing

During the mechanical characterization of fused silica disc substrates with GeNS, many observations were made of an ageing effect worsening the mechanical losses of the samples over time, as it has been shown in Fig. 3.

The ageing seems to increase the difference between the butterfly and the mixed mode families: the first ones have the vibration more and more concentrated towards the edge of the disc as the mode number increases (in Fig. 7 the (m,0) butterfly modes show increasing losses with higher azimuthal nodal lines, m); based on this, a possible explanation of ageing comes from the contamination of the substrates through the rough edge by absorption of impurities and humidity [20].

Considering that both mode dependence and ageing seem to be related to the rough edge surface of the commercial disc-shaped SiO_2 samples, a further check of these hypotheses and a possible solution to both the issues is represented by the *polishing of the edge surface*. This treatment, together with a following annealing at high temperature of the whole sample, can reduce the excess losses arising from the disc edge and would reduce or delete the ageing effect, making the lateral surface less porous and more resistant to contaminants.

In the next section, a facility for the edge polishing is presented.

3. Edge polishing

Samples can either be bought with polished edges, usually mechanically performed by the vendor, or alternatively the edges can be polished with a CO_2 laser after purchasing. We have designed and assembled a facility for the laser polishing of the barrel of commercial samples, to provide fast and reliable localized heating treatments: the heating power is provided by a CO_2 laser beam, delivered to the barrel surface by suitable optics, to obtain an optimally shaped intensity profile that fits with the particular substrate thickness; the sample is housed by a rotating support, allowing the polishing of the barrel at a stable and controlled rate.

In the following, the technique of the CO_2 polishing facility and its main characteristics are shown.

3.1. CO_2 laser polishing facility

The basic idea for a CO_2 laser polishing facility is to use a CO_2 laser beam, with suitable spot dimensions, to heat just the disc barrel at the right temperature, performing a localized annealing of the region of interest.

Therefore, the setup is essentially made up of:

- a *CO_2 laser source* of 20 W or more, because at this wavelength the power is completely absorbed by fused silica substrates, optimizing the hating treatment;
- an *adjusting telescope*, to obtain the right beam size at the sample lateral surface;
- a *full custom rotary stage*, equipped with a step motor, able to rotate the sample during the polishing treatment at the desired velocity, keeping the sample perfectly stable.

To this setup could be added a pair of galvanometer mirrors between the lens and the rotary stage, to bend the CO_2 beam and realize many different heating patterns.

The main part of the polishing facility is the full custom rotary stage. It has been designed with the idea to have a rotary stage small and handy, easy to move, and that allows to keep the samples perfectly aligned and fixed during the polishing procedure. The drawings of the rotary stage are in Fig. 8a, while details are presented in Fig. 8b.

The chosen step motor is an Orientalmotor αstep AR Series FLEX DC power input built-in controller (model AR66AKD-3) that allows to perform movements at desired rate and direction, through a dedicated software. It has been perfectly integrated inside the structure of the the rotary stage, as can be seen in Fig. 8.

A custom shaft has been realized, to be integrated with that of the step motor allowing to put the sample at the desired height. At its top, a polytetrafluoroethylene (PTFE) supporting plate allows to put the sample in place without the surfaces being damaged. The sample is hold in place by two magnets: one inserted in the supporting plate and the other inside a PTFE disc that has to be placed on the top of the sample.

The normal position is at the lower end of the shaft and every time a new sample needs to be centered, the centering tool can be

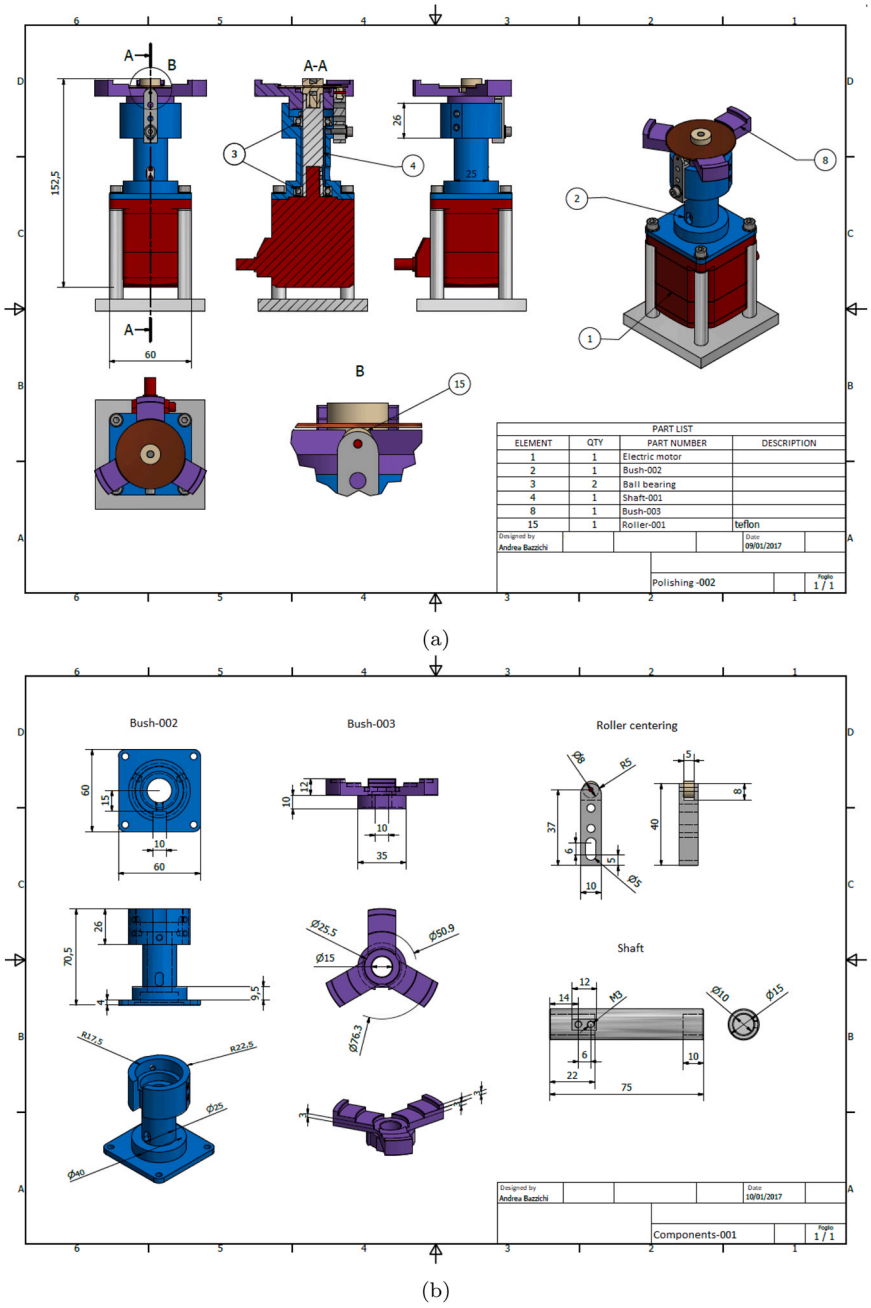

Fig. 8. Rotary stage technical details. (a) Technical design of the rotary stage. (b) Detail of some components of the rotary stage. On the left, the upper part of the rotary stage containing the shaft; in the center, the centering tool in PTFE; on the right, the detail of the support wheel and of the shaft.

shifted up to the required height. It can house sample of one, two or tree inches, and once the sample is blocked by the two PTFE stoppers with the magnets, it can be shifted down (Fig. 9).

The rotary stage has been tested to verify the planar rotation of the samples hold on it: the tolerance with respect to the planar rotation strictly depends on the CO_2 spot dimension and on the dimension of the sample edge to be polished. In Fig. 10a, it is possible to see a scheme of the optical bench layout of the facility for the CO_2 laser polishing of the edge, designed and assembled in the Virgo INFN Roma Tor Vergata laboratory. Here the CO_2 laser beam is pointed to the middle of the sample's edge, using a galvanometer mirror system. It allows single and dual axis movements.

With the Roma Tor Vergata facility it is possible to freely choose a set of parameters to optimize the polishing process and to adapt it to samples with different geometrical dimensions: rotation rate ($v_{rotation}$), number of rounds, applied beam power (P_{laser}) and spot size (w), heating pattern (Fig. 10b). The advantage of having the possibility to choose a pattern depends on the available CO_2 laser power: if the laser is not powerful enough, it will be helpful to reduce the spot size on top of the sample's edge, to have the desired power density, and it can perform some pattern to illuminate the entire thickness of the edge's surface.

Preliminary tests and a polishing campaign on SiO_2 Suprasil® and Corning® substrates, of 1″ and 0.5 mm thickness, and of 2″ and 1 mm thickness, have been performed: in Tab. 2 a summary of the polished samples characteristics is reported.

The effects of this procedure have been quantified both by morphological characterization through atomic force microscope

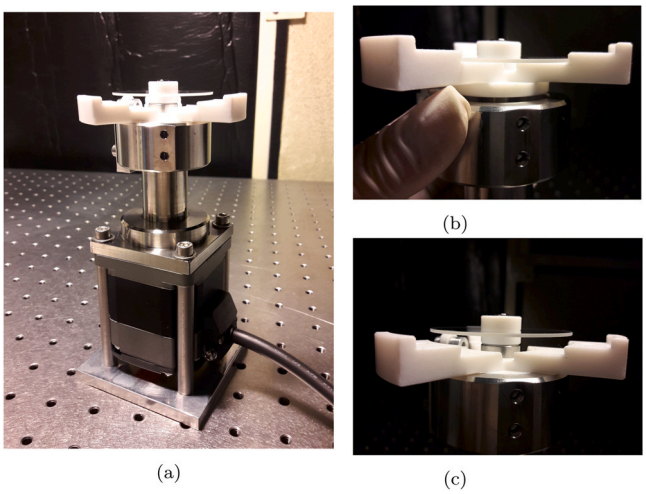

Fig. 9. Pictures of the rotary stage. (a) In the lower part, the αstep motor can be seen, perfectly integrated in the rotary stage structure; in the upper part, a sample (2″ diameter, 1 mm thickness) is mounted on the rotary stage, perfectly aligned with respect to the rotational axis. The PTFE centering tool in the upper, (b), and lower position (c).

(AFM) measurements and through mechanical characterization with GeNS and they are shown in the next section.

4. Results

In this section, the main results of mechanical and morphological characterization of different disc-shaped SiO_2 samples before and after the CO_2 laser polishing of the edge are shown.

The more immediate, visible to the naked eye, result of the sample edge CO_2 laser polishing, is shown in Fig. 11: the initial roughness of edge (Fig. 11a) is visibly reduced after the treatment (Fig. 11b, in this particular case $P_{laser} \sim 15$ W, $w \sim 1$ mm, 4 rounds at a rate of 1/4 of turn per minute).

In the following sections, the morphological and mechanical characterizations for the most significant samples are shown.

4.1. Atomic force microscope characterization

Morphological characterization has been performed by means of atomic force microscopy (AFM). The lateral resolution was of the order of few nanometers, while the vertical resolution was around 1 Angstrom.

Table 2
List of the sample sets involved in the SiO_2 sample preparation procedure study.

material	diam.	thick.	samples number
Corning® 7980	1"	0.5 mm	14
Suprasil® Impex	2"	1 mm	5
No specified fused silica	50 mm	1 mm	14

The AFM available at the Physics department of University of Roma Tor Vergata is a Veeco Multimode (Nanoscope IIIa): Fig. 12a shows the detail of a snippet of the disc edge positioned inside the AFM to be measured.

The first considered sample (2″ diameter and 1 mm thickness) undergoes to a series of tests during the tuning of the CO_2 laser polishing procedure: it has been divided in 16 sections (see Fig. 12b), each of which has been polished with different parameters set (CO_2 laser power, spot dimension, rotation velocity, etc.), to optimize the procedure.

To perform the morphological characterization, the sample has been cut to obtain small snippets compatible with the AFM sample holder.

In Fig. 13 the results of the morphological characterization performed on the best section of the SiO_2 disc-shaped sample mentioned above are shown.

With the optimal parameters (1 mm of spot size for 1 mm of disc thickness and a total power of ~ 9 W) a great reduction of the surface edge roughness has been obtained: it improves by a factor about 250, passing from an initial *RMS* ~ 180 nm to a *RMS* ~ 0.7 nm; in Fig. 13a, also the plane surface of the disc has been morphologically characterized for comparison, showing an *RMS* ~ 2,4 nm. The CO_2 laser polishing technique allows to reach a roughness even better with respect to the sample surface.

4.2. Mechanical loss characterization

The mechanical loss characterization on samples that have been CO_2 laser polished and further annealed has been performed through GeNS and subsequently analysed through a MATLAB® script to extract information about surface loss model parameters. The annealing procedure reduces the residual stresses in the body of the sample and, in addition, allows to loosen the stresses created in the border region by the polishing procedure, as can be seen from an image with polarized light (see Fig. 14): here a polariscope was used to provide a quick and simple assessment of residual stress, not present in the sample under review before the polishing (Fig. 14a) and highlighted by the white line all around the sample's edge after

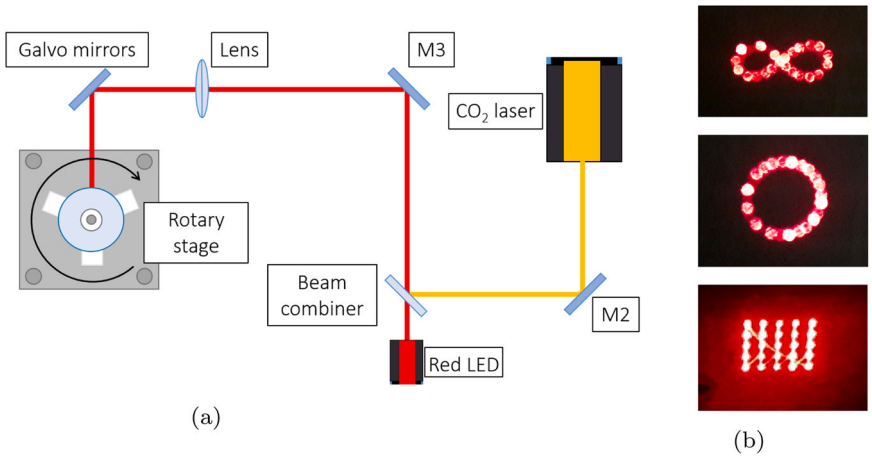

Fig. 10. (a) Optical bench layout of the CO_2 polishing facility in the Roma Tor Vergata INFN laboratory. (b) Three examples of heating pattern achievable with the galvanometer mirrors.

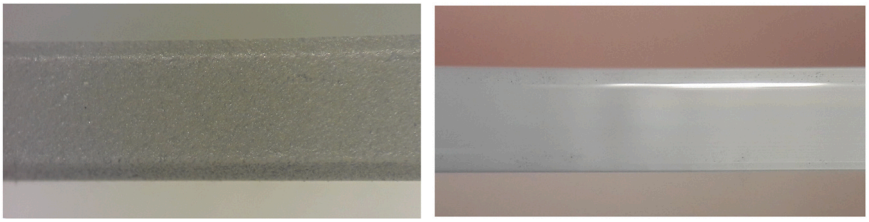

(a) (b)

Fig. 11. Optical microscope photos of a disc edge (1 mm thickness) before (a) and after (b) the CO_2 laser polishing treatment.

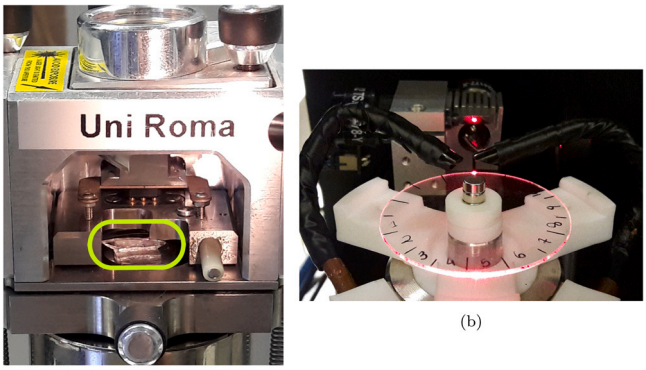

(a) (b)

Fig. 12. (a) The detail of the disc edge snippet (inside the light green circle) that was under measurement; (b) Edge CO_2 laser polishing tests on a disc-shaped sample of 2″ diameter and 1 mm thickness. On the disc many sections are recognizable by a number: each of them corresponds to a different set of CO_2 laser polishing parameters.

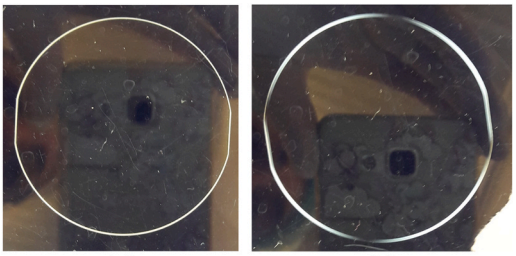

(a) (b)

Fig. 14. Picture through polariscope of a sample before (a) and immediately after (b) CO_2 polishing.

the polishing (Fig. 14b). On some samples also an investigation over time has been performed, to check loss angle sample stability and possible ageing effect.

The two most significant examples are shown: one of the Corning® 7980 samples, of 1" diameter and 0.5 mm thickness (hereafter named CO105001) and one of the Suprasil® Impex samples, 2" diameter and 1 mm thickness (hereafter named SU210001).

In Fig. 15 there are the mechanical characterization of the samples before (a) and (d) and after (b) and (e) the edge CO_2 laser polishing procedure with optimized parameters; the last two plots represented in one case (c) the losses after an annealing at high temperature and in the other case (f) the losses after 10 months, with no particular storage of the sample, that means samples were put in their plastic containers at room temperature in air. The three plots corresponding to the same sample ((a), (b), (c) and (d), (e), (f)) have the same vertical axis scale, to better compare the variation in mechanical losses.

Looking at the blue stars, it is clear that the edge contribution passes from being dominant with respect to the body one (blue dashed lines), to be less relevant, even if still present after CO_2 polishing: the edge component does not always become negligible with the CO_2 laser polishing procedure, the mixed modes remain still distinct with respect to butterfly modes.

For the first considered sample, after the annealing (c), the remaining stresses have been relaxed, the total mechanical losses get even lower and the edge contribution became even less significant, and also the separation between butterfly modes and the mixed one is evidently reduced.

For the second one, the main result achieved is that the CO_2 laser polishing of the edge allows to maintain the sample mechanical losses almost stable in time: the mechanical losses doesn't change in 10 months without any particular storage procedure, showing that the CO_2 laser polishing of the disc edge can reduce or delete the mechanical losses ageing effect, that arises from contaminations. In Fig. 16, the behavior of losses components during time for the

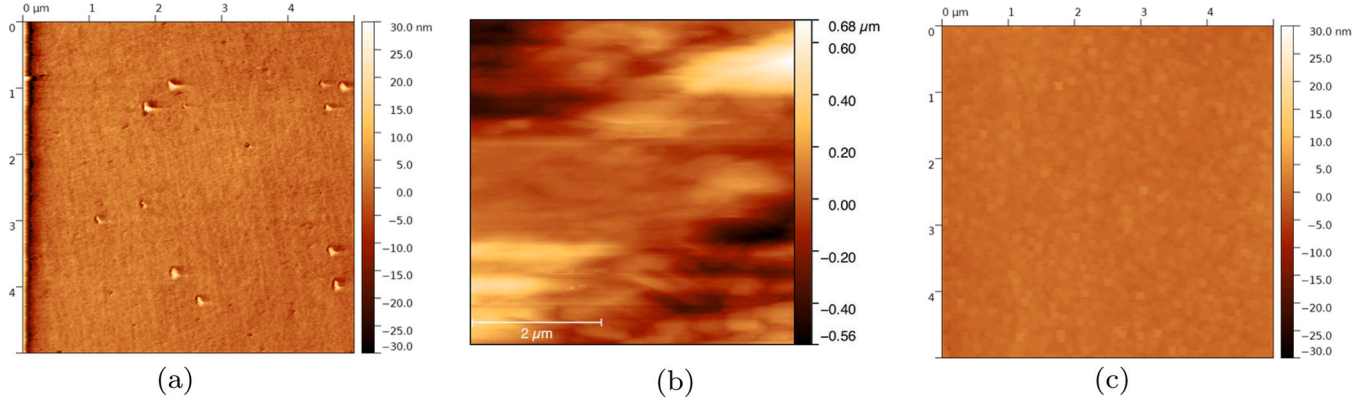

(a) (b) (c)

Fig. 13. AFM measurements of the SiO_2 substrate edge: (a) sample surface; (b) not polished sample edge; (c) polished sample edge. After CO_2 polishing the RMS value fell from 180 nm to 0.7 nm (a reduction of 250 times). Note the different color scale in the images.

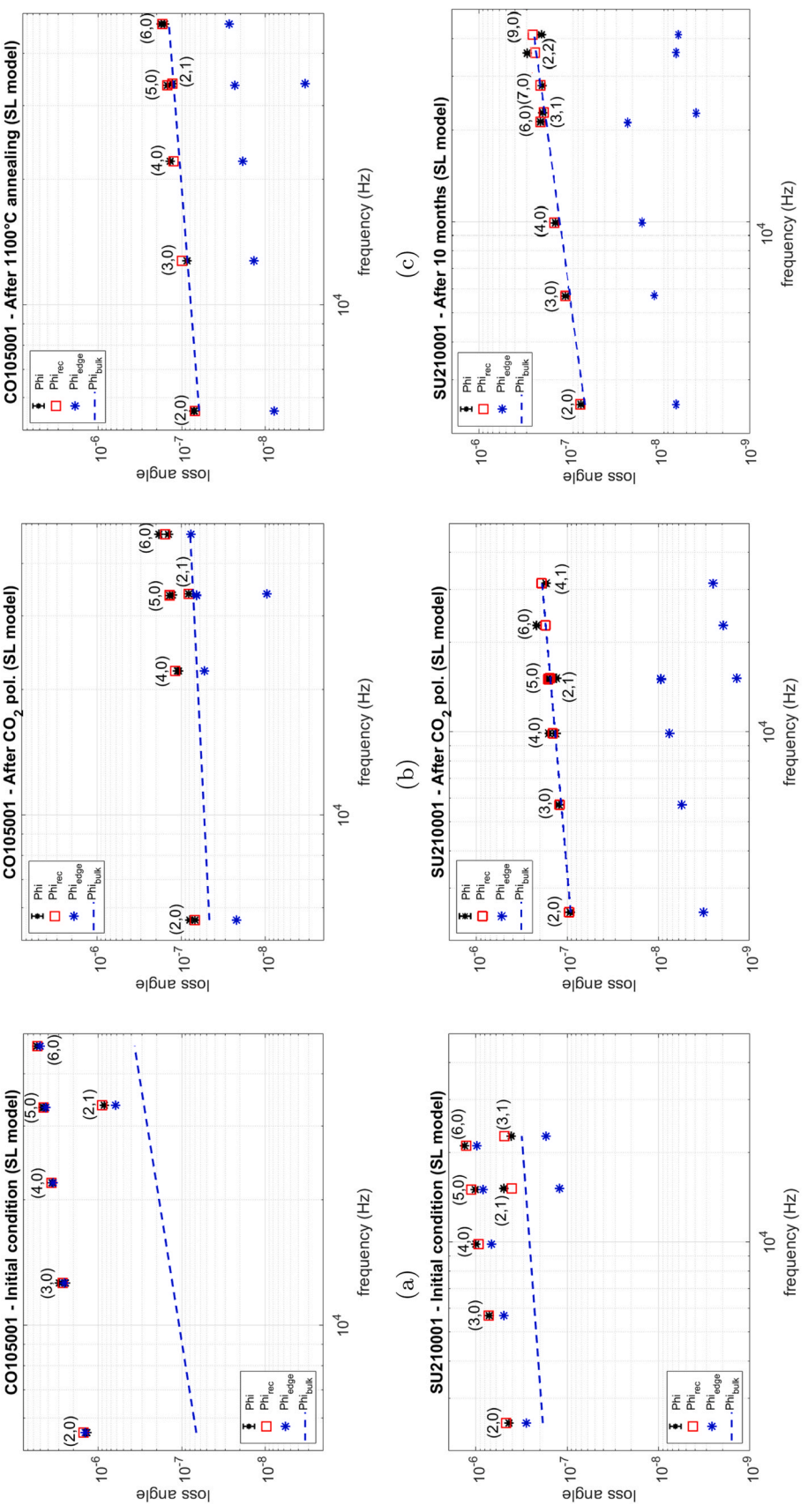

Fig. 15. Mechanical loss measurements and surface loss model application for two samples: (a) (d) Initial mechanical characterization; (b) (e) mechanical characterization after the CO_2 polishing procedure; (c) mechanical characterization after 1100°C annealing; (f) mechanical characterization after 10 months. Black stars are the experimental measurements, red square are the reconstruction of the mechanical losses according to surface loss model, blue stars represent the barrel contribution ($\phi_{barr} = cd\phi_{edge}$), blue dashed line represent the bulk contribution. Note that the vertical axis has the same limits on the three plots corresponding to the same sample.

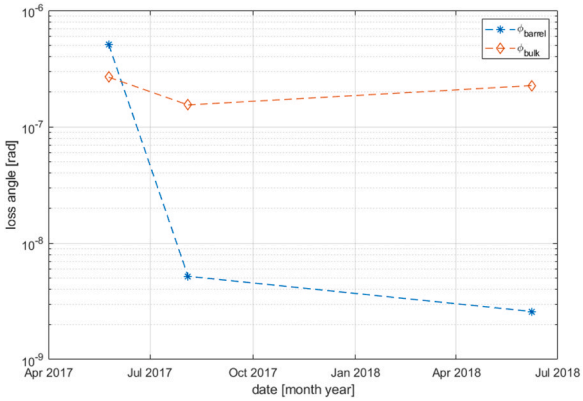

Fig. 16. Behavior of the mechanical losses components after each step for sample SU210001. The bulk contribution remained stable in time inside a reasonable uncertainty.

sample SU210001 are shown: the CO_2 laser polishing drastically reduced the barrel component with respect to the body one, that remains almost stable.

In both cases the general losses reduction is visible:

- for the sample CO105001 the losses reduction is more than one order of magnitude $\Delta\phi_{exp}^{CO_2} \sim -95\%$;
- for the sample SU210001 the losses reduction is less with respect to the other sample, but still significant, being $\Delta\phi_{exp}^{CO_2} \sim -83\%$.

See Tab. 3 for numbers.

Table 3
Mechanical losses summary table for samples considered. ϕ_{exp} is the mean value of the experimental mechanical losses, for which the errors are standard deviations with respect to the mean value; ϕ_{barr} and ϕ_{bulk} are the edge and bulk component of the losses.

Measurement		ϕ_{exp}	ϕ_{barr}	ϕ_{bulk}
CO1050001				
	Initial condition	$(3.3 \pm 1.7) \times 10^{-6}$	3.07×10^{-6}	2.27×10^{-7}
	After CO_2 polishing	$(1.7 \pm 1.7) \times 10^{-7}$	4.94×10^{-8}	6.62×10^{-8}
	After 1100°C annealing	$(1.4 \pm 0.6) \times 10^{-7}$	1.61×10^{-8}	1.10×10^{-7}
SU210001				
	Initial condition	$(7.7 \pm 3.5) \times 10^{-7}$	5.09×10^{-7}	2.67×10^{-7}
	After CO_2 polishing	$(1.3 \pm 0.6) \times 10^{-7}$	5.19×10^{-9}	1.54×10^{-7}
	After 10 months	$(1.8 \pm 0.7) \times 10^{-7}$	9.16×10^{-9}	1.75×10^{-7}

The powerful upgrade with respect to previous way of mechanically characterize SiO_2 substrate is that this edge contribution can be modelled and taken in consideration when substrate's losses are subtracted to estimate the coating loss angle.

5. Conclusions

In this work we highlighted the presence of spurious losses in commercial SiO_2 disc-shaped substrates used in mechanical characterization, aimed at thermal noise reduction in multi-layered coatings for high precision experiments. Both a behavior depending on frequency and excitation modes and a time evolution due to ageing effects were observed and lead back to the ground, unpolished lateral surface. Two models have been used to fit the experimental data: the bulk and shear model, historically used, is not able to model the branching of mechanical losses into family modes; the surface losses model for the bare sample's barrel, instead, is able to reproduce all the loss angle values.

Once identified the origin of these spurious losses in the not polished surface of the disc's edge, a facility for the thermal polishing of this surface was presented and tested.

The CO_2 laser polishing procedure and the facility proposed here showed very good and promising results in terms of mechanical losses stability of SiO_2 substrates.

This procedure must be inserted into the preparation protocol for the substrates to be used in coating mechanical losses characterization: the procedure is easy and reliable, and together with adequate cleaning, annealing treatments and mechanical losses measurements with GeNS, prepares the samples for the deposition of a coating with the coating loss angle estimation goal.

CRediT authorship contribution statement

Diana Lumaca: Conceptualization, Methodology, Software, Validation, Formal analysis, Investigation, Resources, Data curation, Writing – original draft, Writing – review & editing, Visualization. **Alex Amato:** Investigation, Methodology, Visualization, Writing – review & editing. **Matteo Bischi:** Methodology, Investigation, Visualization. **Gianpietro Cagnoli:** Conceptualization, Methodology, Validation, Supervision, Project administration, Writing – review & editing. **Elisabetta Cesarini:** Conceptualization, Methodology, Validation, Supervision, Project administration, Writing – review & editing. **Viviana Fafone:** Project administration, Resources, Funding acquisition. **Massimo Granata:** Investigation, Data curation, Writing – review & editing. **Gianluca Maria Guidi:** Resources, Project administration. **Matteo Lorenzini:** Conceptualization, Methodology, Software, Data curation, Validation, Investigation, Supervision. **Filippo Martelli:** Resources, Project administration. **Lorenzo Mereni:** Resources, Writing – review & editing. **Yury Minenkov:** Resources. **Matteo Montani**: Methodology, Data curation, Investigation, Resources. **Ilaria Nardecchia:** Resources, Supervision, Writing – review & editing. **Francesco Piergiovanni:** Conceptualization, Methodology, Data curation, Validation, Investigation, Resources. **Ernesto Placidi:** Investigation, Data curation, Writing – review & editing. **Alessio Rocchi:** Resources, Funding acquisition.

Data availability

Data will be made available on request.

Declaration of Competing Interest

The authors declare that they have no known competing financial interests or personal relationships that could have appeared to influence the work reported in this paper.

Acknowledgements

The authors want to thanks Andrea Bazzichi and Roberto Simonetti for their precious work on realization and optimization of the first prototype of the rotary stage, main part of the CO_2 laser polishing facility.

This work was promoted by the Virgo Coating R&D (VCR&D) collaboration and supported by University of Roma Tor Vergata, INFN Roma Tor Vergata and European Gravitational Observatory (EGO).

Appendix A. Coating sensitivity

All the efforts to make the substrate losses stable are strictly related to the wish to detect the coating mechanical losses with a certain uncertainty. As already seen in previous sections, it is fundamental to take care about all the effects that can affect fused silica disc-shaped substrate loss angle.

Consider the sensitivity as the ability, in terms of mechanical loss angle, to detect the effect of coating deposition upon a substrate, over the possible variation of the substrate itself. For this reason, the sensitivity condition depends on the substrate's mechanical loss angle or quality factor variation during time:

$$\begin{Bmatrix} \phi_{sub} & \rightarrow \phi'_{sub} \\ Q_{sub} & \rightarrow Q'_{sub} \end{Bmatrix} \tag{A.1}$$

where the variables without and with apex represents the values of the substrate's loss angle and quality factor in two different moments: before and after coating deposition, respectively.

To keep under a certain limit the error in the coating loss, a condition must be imposed on these variations. The relative error on the coating mechanical loss angle evaluation must be smaller than a certain value, that is:

$$\frac{|\Delta\phi_{coat}|}{\phi_{coat}} = \frac{|\phi^{meas}_{coat} - \phi^{true}_{coat}|}{\phi^{true}_{coat}} \leq \eta, \tag{A.2}$$

where η is a small quantity and $\Delta\phi_{coat}$ is the difference between the measured ϕ^{meas}_{coat} and true ϕ^{true}_{coat} values of coating loss angle.

The only available informations are the ones regarding loss angle measurements performed before $\phi_1 = \phi_{sub}$ and after coating deposition $\phi_2 = \phi_{sub+coat}$. The latter one depends on substrate loss angle variation, giving the uncertainty on coating loss angle estimation:

$$\phi_2 = \phi_{sub} + D\phi^{meas}_{coat} = \phi'_{sub} + D\phi^{true}_{coat} = \phi_{sub} + \Delta\phi_{sub} + D\phi^{true}_{coat}, \tag{A.3}$$

where $\Delta\phi_{sub} = \phi' - \phi_{sub}$ is the variation of the substrate's loss angle.

From Eq. (A.3), $\phi^{meas}_{coat} = \phi^{true}_{coat} + \Delta\phi_{sub}/D$ and putting this in Eq. (A.2):

$$\frac{|\Delta\phi_{coat}|}{\phi_{coat}} = \frac{\left|\phi^{true}_{coat} + \frac{\Delta\phi_{sub}}{D} - \phi^{true}_{coat}\right|}{\phi_{coat}} = \frac{|\Delta\phi_{sub}|}{D\phi_{coat}} \leq \eta \tag{A.4}$$

$$\longrightarrow \quad |\Delta\phi_{sub}| \leq \eta D\phi_{coat}, \tag{A.5}$$

or in terms of substrate's quality factors Q:

$$\left|\frac{1}{Q'} - \frac{1}{Q_{sub}}\right| \leq \eta D\phi_{coat} \tag{A.6}$$

Therefore, there are the two following possibilities:

$$\begin{Bmatrix} \text{if } Q_{sub} > Q' \longrightarrow Q' \geq \frac{1}{\frac{1}{Q_{sub}} + \eta D\phi_{coat}} = Q_s^- \\ \text{if } Q_{sub} < Q' \longrightarrow Q' \leq \frac{1}{\frac{1}{Q_{sub}} - \eta D\phi_{coat}} = Q_s^+ \end{Bmatrix} \tag{A.7}$$

Therefore, Q_s^+ and Q_s^- represent the lower and upper limits of quality factor variation that still allows to discern the effect of a coating deposition from the substrate's variation. In Fig. A.1 the two limits are shown in a plot Q' versus Q_{sub}, for a fused silica Corning® 7980 substrate

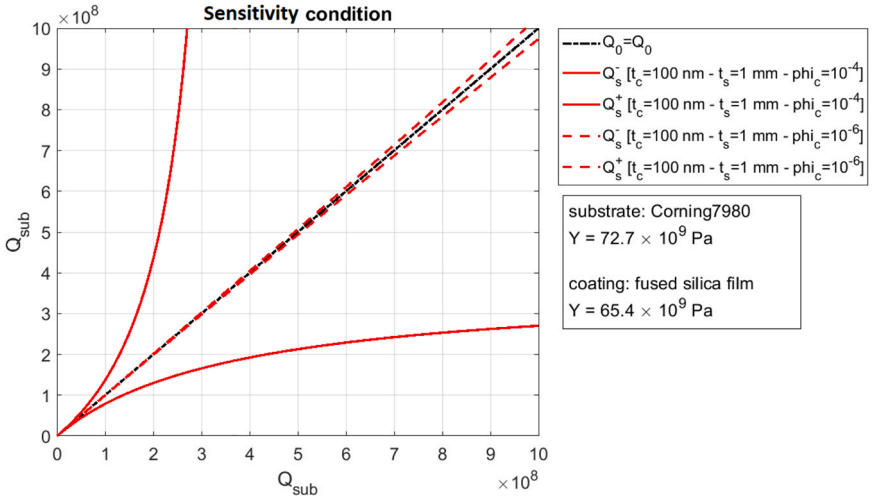

Fig. A. 1. Sensitivity condition for a fused silica Corning® 7980 substrate of 1 mm thickness with a fused silica film coating of 100 nm (and $\eta \sim 0.1$). The variation of the coating loss angle affects significantly the sensitivity condition, reducing drastically the variation of substrate loss angle variation area.

of 1 mm thickness with a fused silica film coating of 100 nm. On the abscissa and on the ordinate axis the value of substrate's quality factor Q_{sub} is represented: a sample whose substrate's quality factor do not change across the coating deposition, is represented by the black dashed line; the two continuous and dashed red lines, instead, represent the two limits between which the substrate's quality factor is allowed to change, not injuring the coating quality factor estimation. For example: a substrate with initial quality factor $\sim 2 \times 10^8$ before a coating film deposition ($\phi_{coat} \sim 10^{-4}$) is allowed to change to not less than $\sim 1.3 \times 10^8$ and no more than $\sim 4.3 \times 10^8$, to allow us to properly detect the coating's mechanical properties. Considering an expected level of coating loss angle of the order of 10^{-4} the substrate losses variation allowed without compromising the coating loss angle evaluation is pretty wide (the area between the two continuous red lines), but the situation change drastically considering a coating loss angle of the order of 10^{-6} (the area between the two dashed red lines). To have a reference, SiO_2 coating films actually used in gravitational wave detectors have mechanical losses of the order of $\sim 5 \times 10^{-5}$ [21].

References

[1] K. Numata, et al., Thermal-noise limit in the frequency stabilization of lasers with rigid cavities, Phys. Rev. Lett. 93 (2004) 250602.
[2] T.J. Kippenberg, K.J. Vahala, Cavity optomechanics: back-action at the mesoscale, Science 321 (5893) (2008) 1172–1176.
[3] R. Miller, et al., Trapped atoms in cavity QED: coupling quantized light and matter, J. Phys. B At. Mol. Opt. Phys. 38 (2005) S551–S565.
[4] H. Callen, T. Welton, Irreversibility and generalized noise, Phys. Rev. 83 (1951) 34.
[5] Y. Levin, Internal thermal noise in the ligo test masses: a direct approach, Phys. Rev. D 57 (1998) 659–663.
[6] S.D. Penn, et al., Frequency and surface dependence of the mechanical loss in fused silica, Phys. Lett. A 352 (2006).
[7] D.R.M. Crooks, et al., Excess mechanical loss associated with dielectric mirror coatings on test masses in interferometric gravitational wave detectors, Class. Quantum Gravity 19 (2002) 883–896.
[8] T. Li, et al., Measurements of mechanical thermal noise and energy dissipation in optical dielectric coatings, Phys. Rev. D 89 (2014).
[9] S.D. Penn, et al., Mechanical loss in tantala/silica dielectric mirror coatings, Class. Quantum Gravity 20 (2003) 2917–2928.
[10] E. Cesarini, et al., A "gentle" nodal suspension for measurements of the acoustic attenuation in materials, Rev. Sci. Instrum. 80 (2009).
[11] G. Cagnoli, et al., Mode-dependent mechanical losses in disk resonators, Phys. Lett. A 382 (2018) 33.
[12] Granata et al., Mechanical Loss in thin SiO_2 disks, VIR0499A-16.
[13] T. Hong, et al., Brownian thermal noise in multilayer coated mirrors, Phys. Rev. D 87 (2013).
[14] M. Abernathy, et al., Bulk and shear mechanical loss of titania-doped tantala, Phys. Lett. A 382 (2018) 2282–2288.
[15] P. Li, Y. Fang, R. Hu, Thermoelastic damping in rectangular and circular micro-plate resonators, J. Sound Vib. 331 (3) (2012) 721–733.
[16] D. Blair, J. Ferreirinho, Thermoelastic effect in niobium at the superconducting transition, Phys. Rev. Lett. 49 (6) (1982) 375–378.
[17] F. Travasso, et al., Low-frequency internal friction in silica glass, Europhys. Lett. 80 (2007).
[18] K.S. Gilroy, W.A. Phillips, An asymmetric double-well potential model for structural relaxation processes in amorphous materials, Philos. Mag. B 43 (5) (1981) 735–746.
[19] Amato A. et al., A Systematic Error in the Internal Friction Measurement of thin Films, Submitted for Publication, 10.48550/arXiv.2209.06106.
[20] B.U. B. Materials, Basic Materials Division, Heraeus Quarzglas GmbH and Co. KG.
[21] M. Granata, et al., Amorphous optical coatings of present gravitational-wave interferometers, Class. Quantum Gravity 37 (2019).